# Light Chain-Dependent Myosin Structural Dynamics in Solution Investigated by Transient Electrical Birefringence

Don Eden and Stefan Highsmith*

*Department of Biochemistry, University of the Pacific, San Francisco, California 94115, and Department of Chemistry and Biochemistry, San Francisco State University, San Francisco, California 94132 USA

ABSTRACT The technique of transient electrical birefringence was used to compare some of the electric and structural dynamic properties of myosin subfragment 1 (S1(elc, rlc)), which has both the essential and regulatory light chains bound, to S1(elc), which has only an essential light chain. The rates of rotational Brownian motion indicate that S1(elc, rlc) is larger, as expected. The permanent electric dipole moment of S1(elc, rlc) is also larger, indicating that the regulatory light chain portion of S1(elc, rlc) has a dipole moment and that it is aligned head-to-tail with the dipole moment of the S1(elc) portion. The permanent electric dipoles decrease with increasing ionic strength, apparently because of ion binding to surface charges. Both S1(elc, rlc) and S1(elc) have intrinsic segmental flexibility, as detected by the ability to selectively align segments with a brief weak electric field. However, unlike S1(elc), which can be structurally distorted by the action of a brief strong electric field, S1(elc, rlc) is stiffer and cannot be distorted by fields as high as 7800 V/cm applied to its ~8000 D permanent electric dipole moment. The S1 · MgADP · $P_i$ analog S1 · MgADP · $V_i$ is smaller than S1 · MgADP, for both S1(elc, rlc) and S1(elc). Interestingly, the smaller, stiffer S1(elc, rlc) · MgADP · $V_i$ complex retains intrinsic segmental flexibility. These results are discussed within a framework of current hypotheses of force-producing mechanisms that involve S1 segmental motion and/or the loss of cross-bridge flexibility during force production.

## INTRODUCTION

Two roles of myosin cross-bridge segmental motion appear in many of the current hypotheses of the mechanical mechanism of force production by the actin-myosin-ATP system. The most common is a reorientation of one segment of myosin subfragment 1 (S1) to produce force while another segment is bound firmly to actin. In some cases this force-producing reorientation is a reversal of a energized S1 conformation produced by ATP binding and/or hydrolysis before S1 · MgADP · $P_i$ binds to actin. The second hypothetical role of segmental motion in force generation is to provide some or all of a high degree of S1 flexibility that exists when S1 first binds to actin and is then lost as S1 becomes more rigid and force is produced. These force-producing transitions are accompanied by the dissociation of the ATP hydrolysis products from the actin-bound S1.

Computer graphical visual docking of S1 on actin, using the atomic structures of actin and S1, provides a complex that has the S1 catalytic domain (which includes the ATP and actin-binding sites) closest to actin and the regulatory domain (which includes the essential and regulatory light chains bound to a long strand of heavy chain $\alpha$-helix) more distant from actin (Rayment et al., 1993a). These high-resolution structural data suggest that if S1 segmental motion is involved in force generation, it is the segment that includes the light chains that is likely to move.

*Received for publication 24 January 1997 and in final form 9 May 1997.*

Address reprint requests to Dr. Stefan Highsmith, Department of Biochemistry, University of the Pacific, 2155 Webster St., San Francisco, CA 94115-2399. Tel.: 415-929-6670; Fax: 415-929-6654; E-mail: shighsmith@uop.edu.



0006-3495/97/08/952/07 $2.00

Indications of segmental motion have been observed for S1-actin complexes. Comparison of image reconstructions from electron micrographs of actin filaments saturated with smooth muscle S1 and S1 · MgADP indicates that only the segment of S1 distal to actin is displaced when ADP is absent (Whittaker et al., 1995). S1 segmental motion in skinned muscle fibers has also been inferred from measurements using orientation-reporting probes attached to the catalytic and regulatory domains. During ATP hydrolysis, probes attached to the myosin catalytic domain (Thomas and Cooke, 1980; Cooke et al., 1982; Fajer, 1994) or to actin itself (Ostap and Thomas, 1991; Naber and Cooke, 1994) do not rotate, in contrast to changes in the orientation of probes attached to the regulatory light chain (Allen et al., 1996; Ling et al., 1996). Although the degree of correspondence between probe and protein motions (Ajtai et al., 1989, 1994), and the effects of nucleotide on contributions from local probe motion (Tanner et al., 1992), can complicate interpretation, the probe data are consistent with segmental motion.

Functional studies support a mechanical role for segmental motion of the regulatory domain. The in vitro velocity of actin translocation by S1 increases progressively as the essential and regulatory light chains are included with the catalytic domain (Lowey et al., 1993), consistent with the 3–4-nm additional length of the regulatory domain per light chain (Rayment et al., 1993b). Experiments using mutant myosin that has an artificial regulatory domain confirm its involvement in the mechanics of force production (Anson et al., 1996). The catalytic domain, by itself, provides very little if any actin translocation, although it has actin-activated ATPase activity (Waller et al., 1995).

There are many reports of segmental motion for isolated S1 preparations. S1 in solution has been shown by transient

electric birefringence (TEB) to display intrinsic segmental flexibility (Highsmith and Eden, 1986) and by fluorescence anisotropy decay spectroscopy (Aguirre et al., 1989), x-ray scattering (Wakabayashi et al., 1992), neutron scattering (Stone et al., 1995), and TEB (Highsmith and Eden, 1990, 1993) to change shape in response to ATP and ATP analog binding. Segmental flexibility of the myosin head has also been shown for myosin filaments (Adhikari et al., 1997). These segmental motions and shape changes have been adequately modeled as bending of S1 near the center of its long axis between the catalytic and regulatory domains.

Much of the important dynamic structural data for S1 shape changes in solution, where the effects of ATP on S1 structure can be studied in greatest detail, were obtained by using S1(elc), which has only an essential light chain bound. This is unfortunate, given the likely importance of the light chain-containing segment of S1 as a lever arm during force production. Reported here are results from TEB measurements used to investigate some of the electrical and dynamic structural properties of isolated S1(elc, rlc) that has both light chains bound, which are compared to results for the smaller S1(elc). S1(elc, rlc) in solution is larger and has a larger, ionic strength-dependent, permanent electric dipole moment. It retains its intrinsic flexibility when free and when converted to the smaller ADP-vanadate complex. Interestingly, the larger S1(elc, rlc), although intrinsically flexible, is stiffer than S1(elc) in response to electromechanical distortion.

## MATERIALS AND METHODS

### Proteins and chemicals

Myosin was isolated from New Zealand rabbit dorsal muscle (Nauss et al., 1969). S1(elc, rlc) was prepared from myosin by using papain (Margossian and Lowey, 1982). S1(elc) was prepared from myosin by using $\alpha$-chymotrypsin (Weeds and Taylor, 1975). In both cases the S1 was purified by size exclusion chromatography (Sephacryl S-400) followed by anion exchange chromatography (DE-52) (Highsmith and Murphy, 1992). S1(elc, rlc) is a mixture with about equal amounts of either essential light chain 1 or essential light chain 2 bound, in addition to the regulatory light chain. S1(elc) is also a mixture, with about equal amounts of S1 with either essential light chain 1 or light chain 2 bound. MgATPase activities at 25°C were 0.050 ± 0.015 $s^{-1}$.

### TEB Instrumentation

The basic instrument and configuration used to measure decay times from partial and steady-state birefringence signals has been described (Elias and Eden, 1981; Highsmith and Eden, 1993). The electric field pulse generator and detection electronics have been modified to better characterize the faster modes expected for segmental and internal dynamics investigations. The photomultiplier has been modified by reducing the number of active dynodes and increasing the potential drop per dynode, while maintaining a comparable gain. Its output is amplified with two Comlinear CLC100 amplifiers with DC-500 MHz bandwidth in series and sent to a LeCroy 6880A transient digitizer with a 0.742 ns sampling interval. Excitation via the cable pulse generator is facilitated by using up to four Tektronix type 113 delay cables in series. These units have subnanosecond rise times, and each can provide a pulse with a length of 120 ns. The system provides a half-microsecond pulse with rise and fall times of less than 1 ns. System rise and decay times are 2 and 3 ns, respectively, when evaluated using water.

For low-ionic-strength solutions with impedances as high as 350 Ω, the Velonex 360 pulse generator can deliver pulses of up to 3300 V, considerably higher than the rated 2500 V into 200 Ω. The fall times are considerably longer, typically 100 ns for an impedance of 400 Ω, rather than the 20 ns for a matched load of 200 Ω using a special coaxial cable with a 185 Ω impedance; so this configuration is not suitable for measuring decay times. However, the higher voltage pulses have permitted the characterization of dipole moment ($\mu_p$) and saturation birefringence ($\Delta n_{SAT}$) from steady-state Kerr experiments. Data were analyzed by fitting the values of solution steady-state birefringence and applied electric field to the equation (O'Konski et al., 1959)

$$\Delta n = \Delta n_{SAT}\{1 - (3(\coth \beta - 1/\beta))/\beta\} \quad (1)$$

where $\Delta n$ is the measured birefringence, $\Delta n_{SAT}$ is the value of the birefringence when the S1 dipole is maximally aligned with the field, and $\beta = \mu_p E/kT$ ($\mu_p$ is the permanent electric dipole moment and $E$ is the electric field). The $\mu_p$ values reported here were calculated from the orientation function values (= $\{1 - (3(\coth \beta - 1/\beta))/\beta\}$ in Eq. 1), which were as large as 0.35 at a field of $1.3 \times 10^6$ V/m in the cell with an electrode spacing of 0.27 cm for S1 in solutions of 1–3 mM ionic strength.

## RESULTS

### S1 hydrodynamic size, specific birefringence, and electric dipole moment

Typical data for S1 alignment to give a steady-state birefringence signal, $\Delta n_{SS}$, by a weak electric field are shown, along with a typical electric field pulse, in Fig. 1. The hydrodynamic size is determined from these data by ana-

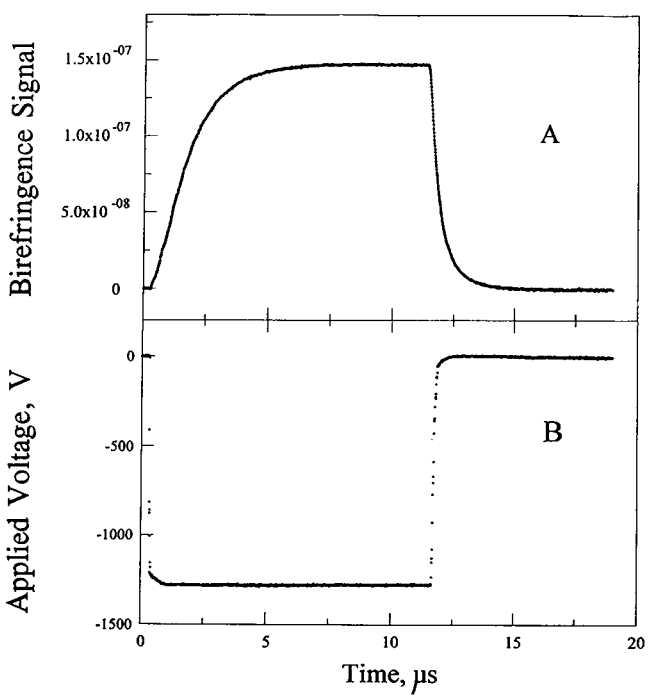


FIGURE 1 Birefringence signal and applied electric field. The birefringence signal, $\Delta n$, (*A*) for 3.18 μM S1(elc, rlc) in 5.0 mM 3-(*N*-morpholino)propanesulfonic acid (MOPS), 10.0 mM KOAc, 0.10 mM $Mg(OAc)_2$, 0.050 mM EGTA, pH 7.0 at 3.7°C when exposed to a 12-μs 1250 V pulse (*B*).

lyzing the rate of decay of $\Delta n$ after the electric field is removed. By using the program DISCRETE (Provencher, 1976), the decay of the birefringence signal, from its steady-state value, for S1(elc, rlc) at 3.5°C was best fit by a single exponential decay with a decay time of 465 ± 3 ns. The decay time for S1(elc) under the same conditions is 316 ± 4 ns (Table 1). In both cases the decay times were independent of ionic strength in the 3–20 mM range. The lengths of S1(elc, rlc) and S1(elc) were estimated from the observed rotational decay times and those for spheres of equal volumes (94.4 ns and 80.4 ns, respectively, at 4°C). Assuming that there is 0.30 g of water bound per gram of protein and that the observed decay times (465 ns and 316 ns, respectively) are due predominantly to rotation about the minor axis, calculations were made, using Perrin shape factors for prolate ellipsoids (Cantor and Schimmel, 1980). For S1(elc, rlc), the length of the hydrated protein was 22.9 nm, with an axial ratio equal to 5.2. For S1(elc), the length and axial ratio were 19.7 nm and 4.5. If the hydration layers are subtracted, the protein lengths are 20.4 nm and 17.6 nm, respectively.

The dependence of the steady-state birefringence signal on the square of the electric field is linear for S1(elc, rlc) for applied voltages between 0 and 2.5 × $10^6$ $V^2$ (Fig. 2). The Kerr constant, determined from the dependence of the birefringence signal on the square of the field (Highsmith and Eden, 1985) in 5.5 mM ionic strength solutions, is 8.1 × $10^{-7}$ $cm^2$/statvolt$^2$. $K_{SP}$ for S1(elc) in 3.0 mM ionic strength is 4.5 × $10^{-7}$ $cm^2$/statvolt$^2$ (Table 1).

The signal for S1(elc, rlc) increases slowly compared to its decay (Fig. 1), indicating that the alignment of S1 in the applied electric field is dominated by the electric field acting on a permanent electric dipole (Tinoco and Yamaoka, 1959; Highsmith and Eden, 1986). The magnitude of the permanent electric dipole moment, $\mu_p$, can be measured by analyzing the data at fields beyond the Kerr law regime, using Eq. 1, as shown in Fig. 3 for S1(elc, rlc). Values of $\mu_p$ = 8100 ± 2000 D and 2452 ± 720 D were obtained for S1(elc, rlc) and S1(elc), respectively, in 1.8–6 mM ionic strength buffer (Table 1).

**TABLE 1 Electric and hydrodynamic properties of S1(elc) and S1(elc,rlc)**

| | S1(elc) | S1(elc,rlc) |
|---|---|---|
| $\tau$ (ns), 10–12 $\mu$s pulse | 316 ± 4 | 465 ± 3 |
| $\tau$ (ns), 0.40 $\mu$s pulse | 250 ± 3 | 414 ± 4 |
| $l$ (nm) | 17.6 ± 0.4 | 20.4 ± 0.5 |
| $\mu_P$ (D) | 2452 ± 720 | 8100 ± 2100 |
| $K_{SP}$ ($cm^2$/statvolt$^2$) | 4.5 ± 0.6 × $10^{-7}$ | 8.1 ± 1.9 × $10^{-7}$ |

Data are for 1–3 $\mu$M S1 at 3.7°C in 1.8–6 mM ionic strength solutions. The length of S1, $l$, is the length of an unhydrated prolate ellipsoid with $\tau$ equal to that observed for S1 after a long pulse. The permanent electric dipole moment, $\mu_P$, was determined from data as shown in Fig. 3. The ionic strengths were 1.8 mM and 2.0 mM for S1(elc,rlc) and S1(elc), respectively. The Kerr constant, $K_{SP}$, was determined from data as shown in Fig. 2. The ionic strengths were 3.0 and 5.5 mM for S1(elc,rlc) and S1(elc), respectively.

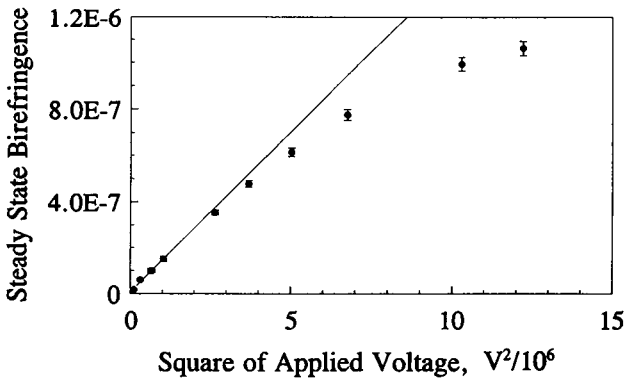


FIGURE 2 Kerr plot for S1(elc, rlc). The steady-state birefringence signal, $\Delta n_{SS}$, obtained for 2.78 $\mu$M S1(elc, rlc) in 5.0 mM MOPS, 0.10 mM $Mg(OAc)_2$, 0.010 mM EGTA, pH 7.0, at 3.7°C, was measured for increasing applied voltages of 12 $\mu$s duration. The birefringence signal in the 11–11.5 $\mu$s region of the applied electric field is averaged and plotted against the square of the applied voltage. The slope of the linear portion of the plot, at low electric field strength, is used to compute the specific Kerr constant, $K_{SP}$, which for the above data is (8.1 ± 1.9) × $10^{-7}$ $cm^2$/statvolt$^2$.

The permanent electric dipole moments of S1(elc, rlc) and S1(elc) decrease as the ionic strength increases (Fig. 4), as does the Kerr constant (data not shown). There were no significant changes in the rise and decay times of the birefringence signal, indicating that the electric dipole moment is permanent in all cases, with negligible induced dipole moment contributions. This observation suggests that as the ionic strength increases, the structure of S1 is changing to one with a smaller electric dipole moment and/or less intrinsic birefringence. Because $\tau$ is independent of ionic strength (see above), S1 does not change its hydrodynamic size. It is possible that as the ionic strength increases, ions are binding to sites on S1. This would neutralize some surface charge, which would reduce the permanent electric dipole moment and possibly change its alignment with respect to the long principal S1 hydrodynamic axis. A

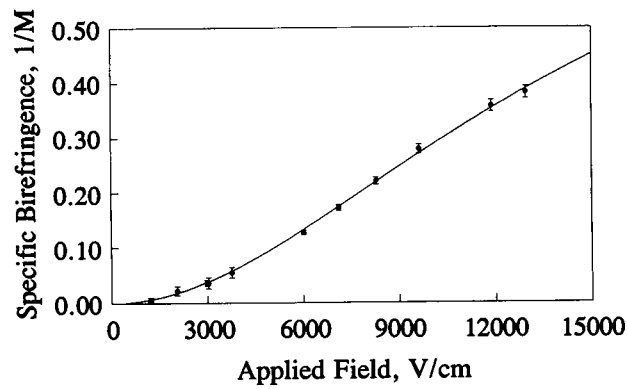


FIGURE 3 Orientation function. The data in Fig. 2 are replotted as specific birefringence, $\Delta n$/[S1], as a function of the applied electric field strength, $E$. The solid line is the best fit to Eq. 1 (see text). The permanent electric dipole moment, $\mu_p$, is 2835 D at 3 mM ionic strength.

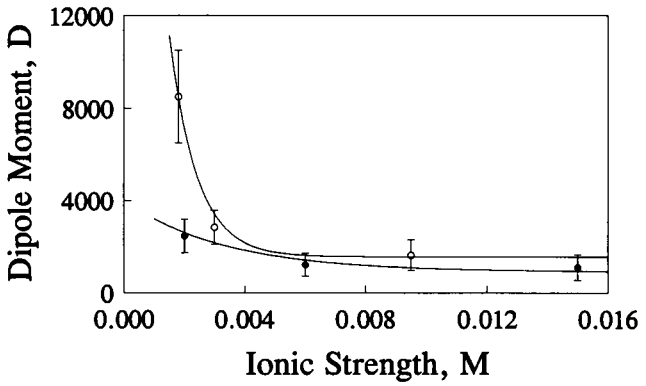


FIGURE 4 Ionic strength dependence of $\mu_P$. The permanent electric dipole moments of S1(elc, rlc) (○) and S1(elc) (●) were determined for solutions of different ionic strengths from the dependence of the measured specific birefringence on the applied electric field (see Fig. 3 for an example). The $\mu_P$ value for S1(elc, rlc) at the lowest ionic strength was determined by using data from an earlier investigation (Highsmith and Eden, 1986).

reduced dipole moment would reduce the Kerr constant, which is consistent with the data.

## S1 segmental flexibility

If a molecular structure includes segments that are displaced by Brownian motion, a short-duration, weak electric field pulse can selectively align those flexibly attached segmental domains. For example, the S1 portions of heavy meromyosin can be selectively aligned by a 0.40 $\mu$s, 3000 V/cm pulse, and their decay resolved from that of the subfragment 2 portion of the molecule, which requires a much longer pulse to produce a significant signal (Highsmith and Eden, 1985). It is not always possible to resolve the segmental decay times. When the rate of motion of the segment is close to the rate of rotation for the whole molecule, the segmental motion and rotation motion are coupled and the decay times are convoluted. However, the relative contribution from the faster segmental motion to the observed signal can be enhanced by using a shorter pulse. It is also possible to observe a shorter relaxation time after a short pulse if the dipole axis and the long principal hydrodynamic axis of rotation are not coincident and if the birefringence is not symmetrical about the long axis. In this case, the rise and decay kinetics can include contributions from rigid body rotation about the shorter axis (Wegener et al., 1979). However, there are many reports indicating that S1 is segmentally mobile (see the Introduction), and it seems likely that the faster decay times observed after short pulses are due to segmental motion, for both S1 and heavy meromyosin (Highsmith and Eden, 1985, 1986).

For S1(elc, rlc), when a 2850 V/cm pulse was shortened from 10 to 0.40 $\mu$s, the single exponential decay decreased from 465 ns to 414 ns, and for S1(elc) the decrease was from 316 ns to 250 ns (Table 1). In an earlier experiment, a decrease in $\tau$ from 320 to 252 ns was observed for S1(elc) when the duration of an applied field was decreased from 7 to 0.4 $\mu$s (Highsmith and Eden, 1990). The decay times for segment motion cannot be resolved, but these results indicate that both S1(elc) and S1(elc, rlc) have flexibly attached segmental domains.

## Structural distortion by electric field-dipole interaction

When the strength of the short-duration electric field pulse applied to S1(elc) is increased above a certain level, further increases in the electric field-free decay rate are observed (Highsmith and Eden, 1986). This field strength dependence of the decay time suggests that, at early stages of the alignment of the components of the total electric dipole moment with a strong enough field, the S1(elc) structure is transiently distorted by the interaction energy of the field and the dipole. When the field is removed, the distorted S1 then "springs back" to its undistorted structure. This recovery from the distortion introduces a deterministic component into the birefringence decay that presumably is not available by thermally driven fluctuations. The additional relaxation mode increases the rate of birefringence decay and decreases the observed decay time.

A decrease in the average decay time is observed for S1(elc) after a 0.40 $\mu$s $E > 3700$ V/cm pulse, but not for S1(elc, rlc) after 0.40 $\mu$s pulses as high as 8100 V/cm (Fig. 5). Because $\mu_P$ is larger for S1(elc, rlc), the interaction energy and distorting force are larger for it than for S1(elc) in an equivalent electric field. It appears that adding the regulatory light chain to S1(elc) stiffens the S1 structure.

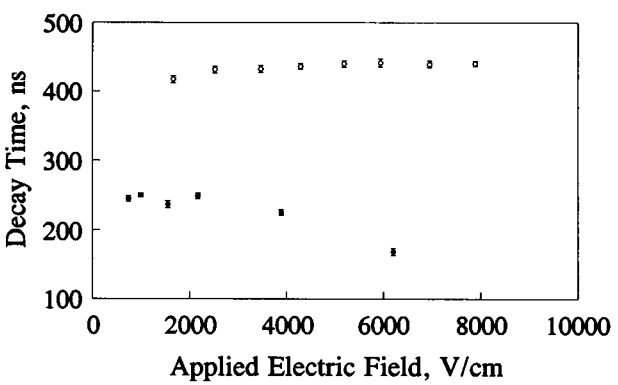


FIGURE 5 Electric field strength dependence of the S1(elc, rlc) and S1(elc) field-free rotational decay times after a short pulse. Solutions of S1 at 3.7°C in 5.0 mM MOPS, 0.10 mM $Mg(OAc)_2$, 0.010 mM EDTA (pH 7.05) were exposed to 0.40 $\mu$s-long applied voltage pulses, and the decay time of the birefringence signal was determined with the program DISCRETE (see text). For S1(elc) (●) the decay time decreases with increasing voltage above 800 V. This reflects the introduction of a deterministic component to the relaxation by the action of the electric field on the S1 permanent electric dipole moment (see text). For S1(elc, rlc) (○), the decay time does not decrease as the applied voltage is increased, within experimental uncertainty, suggesting that the presence of the regulatory light chain stiffens the S1 structure.

### Nucleotide-induced shape changes

It is well established that S1(elc) is converted to a more compact structure when S1(elc) · MgADP · $P_i$ or its analog S1(elc) · MgADP · $V_i$ is formed (Aguirre et al., 1989; Wakabayashi et al., 1992; Highsmith and Eden, 1993; Mendelson et al., 1996). When only MgADP is bound to S1(elc, rlc), the decay time measured by TEB is unchanged within the experimental uncertainty (Highsmith and Eden, 1990). The addition of orthovanadate to S1(elc, rlc) · MgADP to form S1(elc, rlc) · MgADP · $V_i$ reduces the decay time, after a 10 $\mu$s 4630 V/cm pulse, from 468 to 421 ns (Table 2). After a 0.40 $\mu$s pulse, the decay time is reduced from 420 to 371 ns, by the binding of vanadate. The decay time after the longer pulse is smaller for the S1(elc, rlc) · MgADP · $V_i$ complex because it is more compact than S1(elc, rlc) · MgADP · . The additional reduction in decay time after the shorter weak pulse indicates that S1(elc, rlc) · MgADP · $V_i$ retains intrinsic segmental flexibility (Table 2).

Increasing the strength of the short pulse did not decrease the decay time of S1(elc, rlc) · MgADP or S1(elc, rlc) · MgADP · Vi (Fig. 6). The data indicate that S1(elc, rlc), S1(elc, rlc) · MgADP, and S1(elc, rlc) · MgADP · Vi are all too stiff to be distorted by the highest electric field used (see above and Fig. 5).

## DISCUSSION

The presence of the regulatory light chain increases the hydrodynamic size of S1 (Table 1), as expected from its location in the atomic structure of the S1 heterotrimer (Rayment et al., 1993b). Using a prolate ellipsoid as a model for the structure of S1 in solution, the increase in decay time (Table 1) is quantitatively consistent with the 16% increase in the length of S1 estimated from the sizes of the S1(elc) and the regulatory light chain in the atomic structure. This quantitative consistency between the dynamic TEB results and the known static structural properties of S1 supports the validity of the TEB technique for investigating S1 structure.

The presence of the regulatory light chain in S1(elc, rlc) increases the permanent electric dipole moment by 30–300%, depending on the ionic strength (Table 1 and Fig. 4). This result suggests that the permanent electric dipole moment of the regulatory light chain is aligned head-to-tail with that of S1(elc). The exceptionally long stretch of $\alpha$-helix that provided the binding site for both light chains (Rayment et al., 1993b) may contribute a substantial portion of the increase in $\mu_P$ for S1(elc, rlc).

**TABLE 2 Decay times, $\tau$, for S1(elc,rlc) and S1(elc,rlc) · MgADP · $V_i$ after long and short electric field pulses**

| Pulse length, $\mu$s | $-V_i$ | $+V_i$ |
|---|---|---|
| 10 | 468 ± 4 | 421 ± 3 |
| 0.40 | 420 ± 6 | 371 ± 5 |

Data are for 2–3 $\mu$M S1 at 3.7°C in 5.0 mM MOPS, 0.10 mM $Mg(OAc)_2$, 0.010 mM EDTA (pH 7.05). A 1250 V pulse was applied to the sample in a 0.27 cm gap cell.

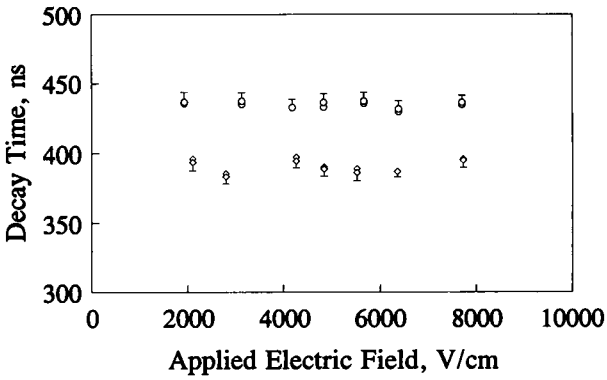


FIGURE 6 Electric field strength dependence of the S1(elc, rlc) · MgADP and S1(elc, rlc) · MgADP · $V_i$ field-free decay times after a short pulse. Solutions of S1(elc, rlc) · MgADP (○) and S1(elc, rlc) · MgADP · $V_i$ (◇) at 3.7°C in 5.0 mM MOPS, 0.10 mM $Mg(OAc)_2$, 0.010 mM EDTA (pH 7.05) were exposed to 0.40 $\mu$s applied voltage pulses, and the decay time of the birefringence signal was determined with the program DISCRETE. Neither complex had a faster decay time for stronger electric field pulses, indicating that, as was the case for S1(elc, rlc), neither S1(elc, rlc) · MgADP · $V_i$ nor S1(elc, rlc) · MgADP is distorted by the action of the electric field on its electric dipole moment. At all field strengths, the rotational decay time for S1(elc, rlc) · MgADP · $V_i$ is smaller than for S1(elc, rlc) or S1(elc, rlc) · MgADP, indicating that the vanadate complex is a more compact structure.

Increased ionic strength decreases both $\mu_P$ (Fig. 4) for both S1(elc, rlc) and S1(elc). These changes in $\mu_P$ are consistent with higher ionic strength reducing electric charge on the surface and/or changing S1 structure. The steady-state value of the birefringence also decreases with increasing ionic strength (data not shown), which is also consistent with both possibilities. Changes in the values of $\Delta n_{SAT}$ might have revealed a structural change, but unfortunately as the dipole changes magnitude, it may also change orientation relative to the molecular axis. However, the rotational decay time for S1(elc, rlc) in the absence of the electric field is ionic strength independent, indicating that the hydrodynamic size of S1 does not change. More subtle shape changes might not be detected, but this result suggests that S1 shape changes are not occurring and favors reduced surface charge as the cause of the reduced $\mu_P$, presumably due to ion binding. Which ions might be binding to S1 cannot be determined from the data. However, this putative ion binding to change the electric dipole moment is consistent with reports that anions bind to S1 to change its net electric charge (Bartels et al., 1993).

The largest dipole moments, observed at the lowest ionic strengths, do not persist at the ionic strengths expected in vivo (Fig. 4). Nonetheless, by extrapolation, an estimate of $\mu_P$ for S1(elc, rlc) in 200 mM ionic strength is still ~1000 D (Fig. 4). Interactions of this large electric dipole moment with electrical charges on the surface of actin in fibers may contribute to positioning the cross-bridge, or to fiber stiffness, in the absence of van der Waals or hydrogen bond

contributions to binding (Banos et al., 1996; Brenner et al., 1996).

The stochastic segmental motion, observed earlier for S1(elc) (Highsmith and Eden, 1986), is retained in the S1(elc, rlc) and S1(elc, rlc) · MgADP cases (Tables 1 and 2). These results suggest that segmental flexibility is an intrinsic structural characteristic of isolated S1 and that it is probably a property of S1 as part of the myosin cross-bridge. The ability to distort the structure of S1 by the application of an increasingly strong short electric field pulse, as observed for S1(elc), is lost when the regulatory light chain is present (Fig. 5). The interaction energies, $U_i = \mathbf{E} \cdot \boldsymbol{\mu}_P$, are larger for S1(elc, rlc), than for S1(elc), because S1(elc, rlc) has a larger $\boldsymbol{\mu}_P$ and was subjected to higher electric fields. It appears that the deterministic contribution to the decay times for S1(elc), which is introduced by field-induced distortion of the structure (Highsmith and Eden, 1986), although interesting, is unlikely to be relevant to the contractile process. The difference in the stiffness of S1(elc) and S1(elc, rlc) detected here suggests that caution should be exercised in applying structural properties measured for S1(elc) to more complete portions of myosin or to myosin itself.

The reduced hydrodynamic size observed for S1(elc) when it forms a MgADP · $V_i$ complex (Highsmith and Eden, 1990) is also observed with S1(elc, rlc) (Table 2). If S1(elc, rlc) · MgADP · $P_i$ is also more compact, as this and several other reports suggest (Aguirre et al., 1989; Highsmith and Eden, 1990, 1993; Wakabayashi et al., 1992; Stone et al., 1995), the S1(elc, rlc) · MgADP · $V_i$ data support models of force generation that have involve unbending of a bent energized cross-bridge as a contributor to the actin-displacing mechanics (Highsmith and Eden, 1990; Rayment et al., 1993a). The displacement of the tip of S1(elc) for the S1(elc) · MgADP · $V_i$ to S1(elc) · MgADP transition, assuming that it bends at its center, was estimated to be 5.2 nm (Highsmith and Eden, 1990). Using the same approach for S1(elc, rlc), the displacement is 6.0 nm, which is the distance that actin would be moved by the conformational change associated with $V_i$ (and perhaps $P_i$) dissociation, if it occurred while S1 was bound to actin.

It is interesting that the stochastic flexibility is retained when $V_i$ is bound to produce the smaller S1(elc, rlc) · MgADP · $V_i$ (Table 2). The internal motions of S1 backbone and side chains, monitored by proton NMR linewidth, also persist when S1 · MgADP · $P_i$ forms, and are only frozen out by actin binding (Highsmith et al., 1979). Again assuming that S1 · MgADP · $V_i$ is an analog of S1 · MgADP · $P_i$, binding of an internally mobile and segmentally flexible intermediate to actin first is consistent with models of force production that involve a disorder-to-order transition (Hambly et al., 1991; Raucher and Fajer, 1994; Thomas et al., 1995).

Supported by National Institutes of Health grants AR42895 (to SH) and AR42751 (to DE). A preliminary report of these data appeared in the Seventh Biophysical Discussions, *Biophys. J.* 68:372S–373S (1995).

## REFERENCES

Adhikari, B., K. Hildeg, and P. G. Fajer. 1997. Independent domain mobility of myosin heads in myosin filaments as determined by STEPR. *Proc. Natl. Acad. Sci. USA.* in press.

Aguirre, R., S. H. Lin, F. Gonsoulin, C. K. Wang, and H. C. Cheung. 1989. Characterization of the ethenoadenosine diphosphate binding site of myosin subfragment 1. Energetics of the equilibrium between two states of nucleotide-S1 and vanadate-induced global conformation changes detected by energy transfer. *Biochemistry.* 28:799–807.

Ajtai, K., A. R. French, and T. P. Burghardt. 1989. Myosin cross-bridge orientation in rigor and in the presence of nucleotide studied by electron spin resonance. *Biophys. J.* 56:535–541.

Ajtai, K., D. J. Toft, and T. P. Burghardt. 1994. Path and extent of cross-bridge rotation during muscle contraction. *Biochemistry.* 33: 5382–5391.

Allen, T. S., N. Ling, M. Irving, and Y. E. Goldman. 1996. Orientation changes in myosin regulatory light chains following photorelease of ATP in skinned muscle fibers. *Biophys. J.* 70:1847–1862.

Anson, M., M. A. Geeves, S. E. Kurzawa, and D. J. Manstein. 1996. Myosin motors with artificial lever arms. *EMBO J.* 15:6069–6074.

Banos, F. G. D., J. Bordas, J. Lowy, and A. Svenssen. 1996. Small segmental rearrangements in the myosin head can explain force generation in muscle. *Biophys. J.* 71:576–589.

Bartels, E. M., P. H. Cooke, G. F. Elliott, and R. A. Hughes. 1993. The myosin molecule—charge response to nucleotide binding. *Biochim. Biophys. Acta.* 1157:63–73.

Brenner, B., S. Xu, J. M. Chalovich, and L. C. Yu. 1996. Radial equilibrium lengths of actomyosin cross-bridges in muscle. *Biophys. J.* 71: 2751–2758.

Cantor, C. R., and P. R. Schimmel. 1980. Macromolecules as Hydrodynamic Particles. *In* Biophysical Chemistry. A. C. Bartlett, editor. Freeman and Co., San Francisco. 562–565.

Cooke, R., M. S. Crowder, and D. D. Thomas. 1982. Orientation of spin labels attached to cross-bridges in contracting muscle fibres. *Nature.* 300:776–778.

Elias, J. G., and D. Eden. 1981. Transient electric birefringence study of the persistence length and electrical polarizability of restriction fragments of DNA. *Macromolecules.* 14:410–419.

Fajer, P. G. 1994. Method for the determination of myosin head orientation from EPR spectra. *Biophys. J.* 66:2039–2050.

Hambly, B., K. Franks, and R. Cooke. 1991. Orientation of spin-labeled light chain-2 exchanged onto myosin cross-bridges in glycerinated muscle fibers. *Biophys. J.* 59:127–138.

Highsmith, S., K. Akasak, M. Konrad, R. Goody, K. Holmes, N. Wade-Jardetzky, and O. Jardetzky. 1979. Internal motions in myosin. *Biochemistry.* 18:4238–4244.

Highsmith, S., and D. Eden. 1985. Transient electrical birefringence characterization of heavy meromyosin. *Biochemistry.* 24:4917–4924.

Highsmith, S., and D. Eden. 1986. Myosin subfragment 1 has tertiary structural domains. *Biochemistry.* 25:2237–2242.

Highsmith, S., and D. Eden. 1990. Ligand-induced myosin subfragment 1 global conformational change. *Biochemistry.* 29:4087–4093.

Highsmith, S., and D. Eden. 1993. Myosin-ATP chemomechanics. *Biochemistry.* 32:2455–2458.

Highsmith, S., and A. J. Murphy. 1992. Electrostatic changes at the actomyosin-subfragment 1 interface during force-generating reactions. *Biochemistry.* 31:385–389.

Ling, N., C. Shrimpton, J. Sleep, J. Kendrick-Jones, and M. Irving. 1996. Fluorescent probes of the orientation of myosin regulatory tight chains in relaxed, rigor, and contracting muscle. *Biophys. J.* 70:1836–1846.

Lowey, S., G. S. Waller, and K. M. Trybus. 1993. Skeletal muscle myosin light chains are essential for physiological speeds of shortening. *Nature.* 365:454–456.

Margossian, S. S., and S. Lowey. 1982. Preparation of myosin and its subfragments from rabbit skeletal muscle. *Methods Enzymol.* 85:55–71.

Mendelson, R. A., D. K. Schneider, and D. B. Stone. 1996. Conformations of myosin subfragment 1 ATPase intermediates from neutron and X-ray scattering. *J. Mol. Biol.* 256:1–7.

Naber, N., and R. Cooke. 1994. Mobility and orientation of spin probes attached to nucleotides incorporated into actin. *Biochemistry.* 33: 3855–3861.

Nauss, K. M., S. Kitagawa, and J. Gergely. 1969. Pyrophosphate binding to and adenosine triphosphatase activity of myosin and its proteolytic fragments. *J. Biol. Chem.* 244:755–765.

O'Konski, C. T., K. Yoshioka, and W. H. Orttung. 1959. Electric properties of macromolecules. IV. Determination of electric and optical parameters from saturation of electric birefringence in solutions. *J. Phys. Chem.* 63:1558–1565.

Ostap, E. M., and D. D. Thomas. 1991. Rotational dynamics of spin-labeled F-actin during activation of myosin S1 ATPase using caged ATP. *Biophys. J.* 59:1235–1241.

Provencher, S. W. 1976. An eigenfunction expansion method for the analysis of exponential decay curves. *J. Chem. Phys.* 64:2772–2777.

Raucher, D., and P. G. Fajer. 1994. Orientation and dynamics of myosin heads in aluminum fluoride induced pre-power stroke states: an EPR study. *Biochemistry.* 33:11993–11999.

Rayment, I., H. M. Holden, M. Whittaker, C. B. Yohn, M. Lorenz, K. C. Holmes, and R. A. Milligan. 1993a. Structure of the actin-myosin complex and its implications for muscle contraction. *Science.* 261: 58–65.

Rayment, I., W. R. Rypniewski, K. Schmidt-Base, R. Smith, D. R. Tomchick, M. M. Benning, D. A. Winkelmann, G. Wesenberg, and H. M. Holden. 1993b. 3-Dimensional structure of myosin subfragment-1—a molecular motor. *Science.* 261:50–58.

Stone, D. B., D. K. Schneider, Z. W. Huang, and R. A. Mendelson. 1995. The radius of gyration of native and reductively methylated myosin subfragment-1 from neutron scattering. *Biophys. J.* 69:767–776.

Tanner, J. W., D. D. Thomas, and Y. E. Goldman. 1992. Transients in orientation of a fluorescent cross-bridge probe following photolysis of caged nucleotides in skeletal muscle fibres. *J. Mol. Biol.* 223:185–203.

Thomas, D. D., and R. Cooke. 1980. Orientation of spin-labeled myosin heads in glycerinated muscle fibers. *Biophys. J.* 32:891–906.

Thomas, D. D., S. Ramachandran, O. Roopnarine, D. W. Hayden, and E. M. Ostap. 1995. The mechanism of force generation in myosin: a disorder-to-order transition, coupled to internal structural changes. *Biophys. J.* 68:135s–141s.

Tinoco, J. R., I, and K. Yamaoka. 1959. The reversing pulse technique in electric birefringence. *J. Phys. Chem.* 63:423–427.

Wakabayashi, K., M. Tokunaga, I. Kohno, Y. Sugimoto, T. Hamanaka, Y. Takezawa, T. Wakabayashi, and Y. Amemiya. 1992. Small-angle synchrotron x-ray scattering reveals distinct shape changes of the myosin head during hydrolysis of ATP. *Science.* 258:443–447.

Waller, G. S., G. Ouyang, J. Swafford, P. Vibert, and S. Lowey. 1995. A minimal motor domain from chicken skeletal muscle myosin. *J. Biol. Chem.* 270:15348–15352.

Weeds, A. G., and R. S. Taylor. 1975. Separation of subfragment-1 isoenzymes from rabbit skeletal muscle myosin. *Nature.* 257:54–56.

Wegener, W. A., R. M. Dowben, and V. J. Koester. 1979. Time-dependent birefringence, linear dichroism and optical rotation resulting from rigid body rotational diffusion. *J. Chem. Phys.* 70:622–632.

Whittaker, M., E. M. Wilson-Kubalek, J. E. Smith, L. Faust, R. A. Milligan, and H. L. Sweeney. 1995. A 35-angstrom movement of smooth muscle myosin on ADP release. *Nature.* 378:748–751.